INDERSCIENCE PUBLISHERS
Linking academia, business and industry through research

International Journal of Data Mining and Bioinformatics

ISSN online: 1748-5681 - ISSN print: 1748-5673
https://www.inderscience.com/ijdmb

Hypertension-driven mechano-immune crosstalk related novel genes may be potential targets for IA rupture progression

Ji-Yun Liu, Jun Yuan, Li Luo, Xuan Yin

DOI: 10.1504/IJDMB.2026.10075327

Article History:

Received:	17 July 2025
Accepted:	25 November 2025
Published online:	07 January 2026

Hypertension-driven mechano-immune crosstalk related novel genes may be potential targets for IA rupture progression

Ji-Yun Liu, Jun Yuan and Li Luo

Department of Clinical Laboratory,
Guiyang Second People's Hospital,
Guiyang, China
Email: liujiynu2093@163.com
Email: 1760075125@qq.com
Email: 514884295@qq.com

Xuan Yin*

Department of Women Healthcare,
Guiyang Maternal and Child Healthcare Hospital,
Guiyang, China
Email: yinxuan0517@163.com
*Corresponding author

Abstract: Integrated genomic and transcriptomic analyses were employed to identify novel molecular targets and elucidate underlying mechanisms in the progression from unruptured to ruptured intracranial aneurysms (IAs). The study integrated differentially expressed genes identified through GWAS-based SNP screening and transcriptomic analysis of three independent datasets (GSE13353, GSE26969, GSE75436). Protein-protein interaction network construction and functional enrichment analysis of overlapping genes revealed two key interactions: ITGAX-JAM3 and KLHL28-TOGARAM1, with ITGAX and MAGI2 emerging as consensus genes across all datasets. Machine learning-based prioritisation via LASSO regression with L1 penalty selected optimal characteristic genes, validated through ROC curve analysis (AUC > 0.85). These findings demonstrate that ITGAX, JAM3, KLHL28, TOGARAM1, and MAGI2 represent promising molecular targets worthy of further investigation in the context of hypertension-driven mechano-immune crosstalk during IA rupture progression, providing new insights for both mechanistic studies and clinical management strategies.

Keywords: intracranial aneurysm; hypertension; immunity; single-nucleotide polymorphisms; bioinformatics.

Reference to this paper should be made as follows: Liu, J-Y., Yuan, J., Luo, L. and Yin, X. (2026) 'Hypertension-driven mechano-immune crosstalk related novel genes may be potential targets for IA rupture progression', *Int. J. Data Mining and Bioinformatics*, Vol. 30, No. 5, pp.1–14.

Biographical notes: Ji-Yun Liu is an Associate Senior Clinical Laboratory Technician experienced in molecular genetics and laboratory quality management.

Jun Yuan is the Director of the Prenatal Diagnosis Center, a PhD and chief technician leading research in microbiology and immunology.

Li Luo is an Associate Chief Technician specialising in molecular and genetic testing, with advanced training in cytogenetics.

Xuan Yin is a maternal healthcare physician involved in major birth cohort studies and the development of clinical guidelines.

1 Introduction

Intracranial aneurysms (IAs) are pathological expansions of the cerebral arterial wall that pose a serious concern in neurosurgery, primarily because of their risk of rupture and the possibility of resulting subarachnoid hemorrhage (SAH) (Etminan and Rinkel, 2016). Improvements in the quality and availability of neuroimaging techniques have led to an increase in the worldwide detection frequency of IAs, which is now estimated at roughly 6.1 per 100,000 person-years (Etminan et al., 2019). Understanding the mechanisms underlying unruptured intracranial aneurysm (UIA) formation and rupture is essential for reducing societal and familial burdens. The formation of IAs is a multifactorial and gradual process, driven by hemodynamic forces (Kassam et al., 2004) and predisposing conditions including hypertension, dyslipidemia, atherosclerosis, and smoking (Frösen et al., 2013, 2012; Etminan et al., 2014), and genetic predisposition (Bor et al., 2014).

The inherent fragility of cerebral arteries – characterised by the absence of an external elastic lamina and sparse medial smooth muscle – predisposes these vessels to pathological dilation. A key pathological step in IA formation involves the breakdown or loss of integrity of the internal elastic lamina, especially in regions of arterial branching (Bor et al., 2008). Hypertension exacerbates this vulnerability through two synergistic pathways:

1 direct mechanical stress from elevated blood pressure weakens the aneurysm wall, with transient spikes (such as during straining, caffeine overconsumption, or intense exercise) inducing irreversible microstructural damage at bifurcation sites (Vlak et al., 2011)

2 Systemic high blood pressure stimulates the tissue renin-angiotensin system, which in turn promotes inflammatory responses and structural changes in the vessel wall (Muller et al., 2004).

While hypertension is recognised as a high-risk driver of IA rupture, its precise molecular contributions remain incompletely defined. This study focuses on the transition from UIA to ruptured IA, leveraging transcriptomic profiling and LASSO regression with L1 regularisation to identify stage-specific biomarkers. We report the first identification of ITGAX, JAM3, KLHL28, TOGARAM1, and MAGI2 as potential mediators of IA rupture. These findings lay a molecular foundation for exploring hypertension-driven mechano-immune crosstalk and developing dual-action therapeutic strategies that integrate antihypertensive and anti-inflammatory properties.

2 Materials and methods

2.1 Construction of flowchart

The study workflow is illustrated in Figure 1. Summary statistics for UIA (ebi-a-GCST90018816) and IA (ebi-a-GCST90018815) were retrieved from the IEU Open GWAS Project (https://gwas.mrcieu.ac.uk/). Differentially expressed single nucleotide polymorphisms (SNPs) were identified and matched with the DbSNP database to generate the 'Diff_Snp_Genes' dataset. Three GEO datasets (GSE13353, GSE26969, and GSE75436 all from https://www.ncbi.nlm.nih.gov/gds/) were analysed, comprising 55 samples (29 cases vs. 26 controls). Differential expression analysis was performed using R software (version 4.4.0) to identify distinct differential expressed genes (DEGs) for each dataset. The 'Diff_Snp_Genes' dataset was intersected with DEGs from the three GEO datasets, resulting in 31 hub genes. Further intersection across all four datasets revealed two shared genes. Functional enrichment analyses (gene ontology [GO], Kyoto Encyclopedia of genes and genomes [KEGG]) and protein-protein interaction (PPI) network construction were conducted on hub genes. TF-miRNA coregulatory interactions were mapped for core genes with significant PPI connections and shared genes. Least absolute shrinkage and selection operator (LASSO) regression was employed to develop a predictive model for UIA-to-IA progression using the identified genes. Model performance was evaluated by using receiver operating characteristic (ROC) curves. As all datasets were sourced from publicly available repositories, no additional ethical approval was required.

2.2 Data processing and differentially expressed gene screening

Differentially expressed SNPs were firstly identified using the 'dplyr' package and annotated against the DbSNP database to generate the 'Diff_Snp_Genes' dataset. Subsequently, gene expression profiles from the GSE13353, GSE26969, and GSE75436 datasets performed log2 transformation. Differential gene expression analysis was performed through using the 'limma' and 'hgu133plus2.db' packages, resulting in three distinct DEGs datasets. Statistically significant DEGs (p-values < 0.05) were defined by thresholds of the |logFC| > (mean (abs (logFC)) + 2*sd (abs (logFC))). In addition, chromosomal density distributions of differentially expressed SNPs were visualised using the 'CMplot' package, represented as SNP density plots and circular Manhattan plots. DEGs were visualised in the form of heatmaps and volcanos through the 'pheatmap' and 'ggplot2' packages.

2.3 Hub genes and shared genes identification

The genes subjected to downstream analyses were categorised into two parts: hub genes and shared genes.

- Hub genes identification: the 'Diff_Snp_Genes' dataset was sequentially intersected with DEGs from the GSE13353, GSE26969, and GSE75436 datasets, generating three differentially overlapping gene sets. These gene sets were subsequently performed to a union operation with deduplication.

- Shared genes identification: shared genes were defined as the common intersection across all four datasets: 'Diff_Snp_Genes' and DEGs from the three GEO datasets (GSE13353, GSE26969, GSE75436). The overlap relationships among the four datasets were finally visualised by using Venn diagram (https://www.bioinformatics.com.cn/).

Figure 1 The flowchart of present study

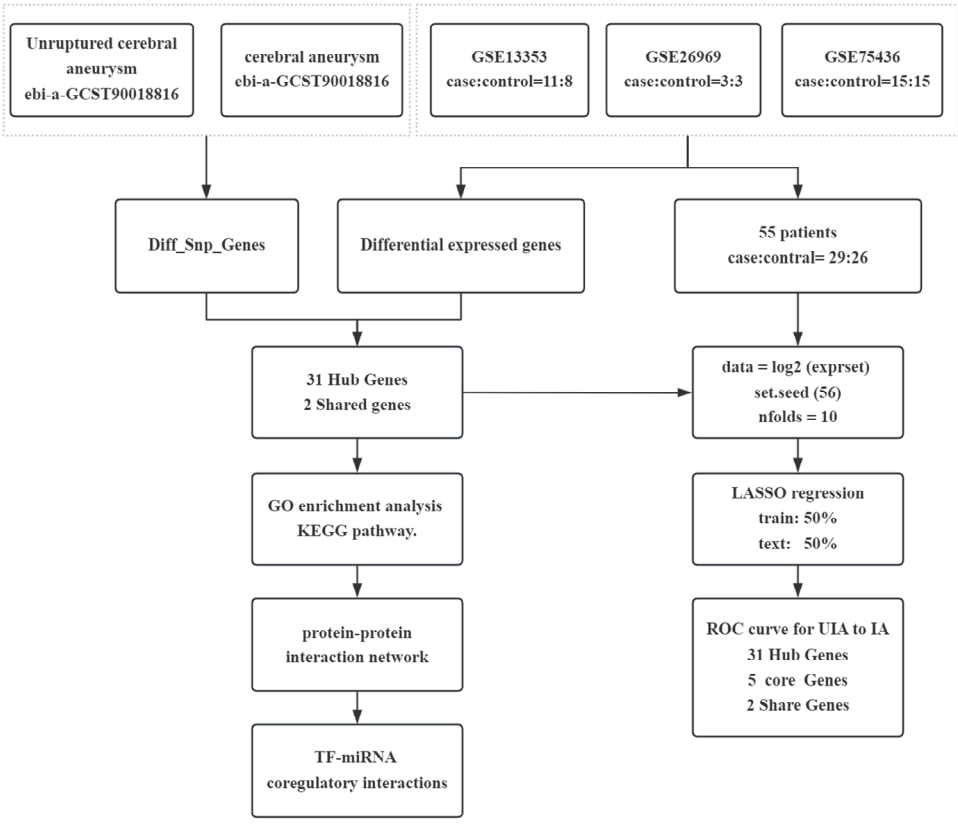

2.4 Functional annotation and construction of genes interaction network

To further clarify the functional enrichment role of these hub genes, we performed GO enrichment and KEGG pathway analyses using the 'clusterProfiler' package. Adjusted p-values < 0.05 were considered statistically significant. GO analysis results were visualised as bubble plots through the 'dotplot' function, while KEGG pathways analysis results were represented as bar plots using 'barplot' function. In addition, hub genes were employed to construct a PPI network (confidence level > 0.4) by using the STRING database (version 12.0, https://string-db.org) (Huang et al., 2024). Genes with significant interactions were retained for downstream analyses. In addition, to reveal the potential regulators of UIA-to-IA progression, these interactional genes and shared genes were amalgamated and employed to build a construction of TF-miRNA coregulatory network, performing by using the Reg-Network database within the Network Analyst platform

(v3.0, https://www.networkanalyst.ca/NetworkAnalyst). finally, this network was visualised by Cytoscape (v3.10.2).

2.5 LASSO regression predictive modelling

LASSO regression, a regularisation method derived from linear regression, was employed to analyse high-dimensional genomic data. Features included the identified hub genes, interactional genes, and shared genes at present study. Data standardisation and model construction were performed using the 'caret', 'glmnet', and 'pROC' packages. Under fixed reproducibility conditions (set.seed = 56), a 10-fold cross-validation framework (nfolds = 10) was applied to optimise the regularisation parameter (λ). A total of 55 samples (29 IA cases vs. 26 controls) were randomly divided into training and test sets at a 50:50 ratio. ROC curves were applied to quantify the predictive ability of distinct gene sets in distinguishing UIA-to-IA progression. Predictive outcomes from the three gene subsets (hub genes, core genes [interactional genes + shared genes], and shared genes) were visualised to assess their predictive power.

2.6 Statistical analysis

All statistical analyses and visualisations were performed using R version 4.4.0.

Figure 2 The SNPs within the IA rupture progression, (a) the SNP density plots showed the chromosomal regions enriched with SNPs implicated in IA rupture, (b) circular Manhattan plots showed the number of SNPs in IA rupture (see online version for colours)

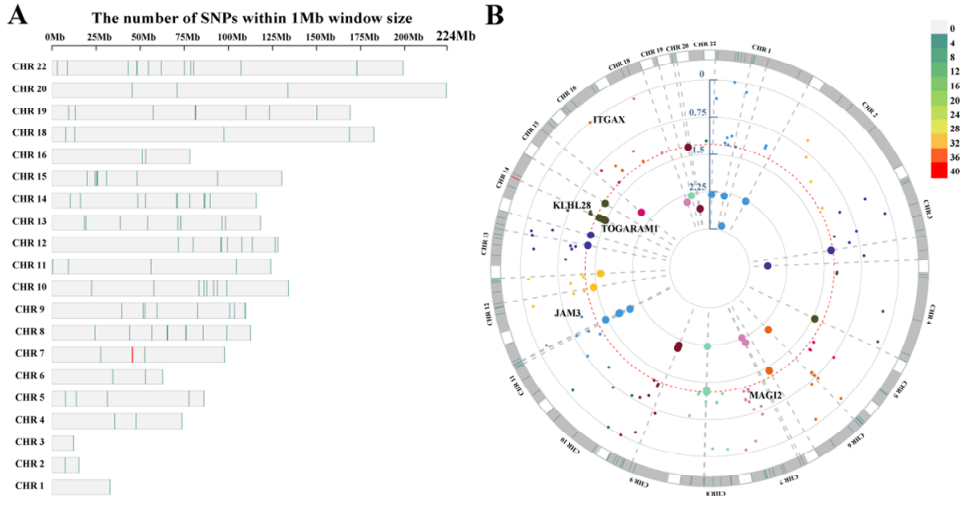

Notes: (a) The x-axis corresponds to the chromosomal base pair coordinates of the SNPs.
(b) The circular perimeter represented the x-axis. The y-axis quantified statistical significance using the –log10(p-value) scale.

3 Results

3.1 Identification of all four differentially expressed gene sets

Four distinct differential gene datasets were established in this study: 'Diff_Snp_Genes,' 'GSE13353 DEGs,' 'GSE26969 DEGs,' and 'GSE75436 DEGs.' The 'Diff_Snp_Genes' dataset was derived from comparative analysis of the UIA and IA GWAS statistical results, identifying 202 SNPs associated with IA rupture. Chromosomal distribution of these SNPs was visualised using SNP density plots [Figure 2(a)]. Subsequently, annotation from the DbSNP database mapped these SNPs to 75 genes, with circular Manhattan plots illustrating 'core genes' identified in downstream analyses [Figure 2(b)].

Figure 3 Visualisation results of differential analyses within IA rupture progression, (a) the heatmap of differentially expressed genes for GSE13353, (b) GSE26969, (c) GSE75436, (d) GSE13353, (e) GSE26969, (f) the volcano of differentially expressed genes for GSE75436 (see online version for colours)

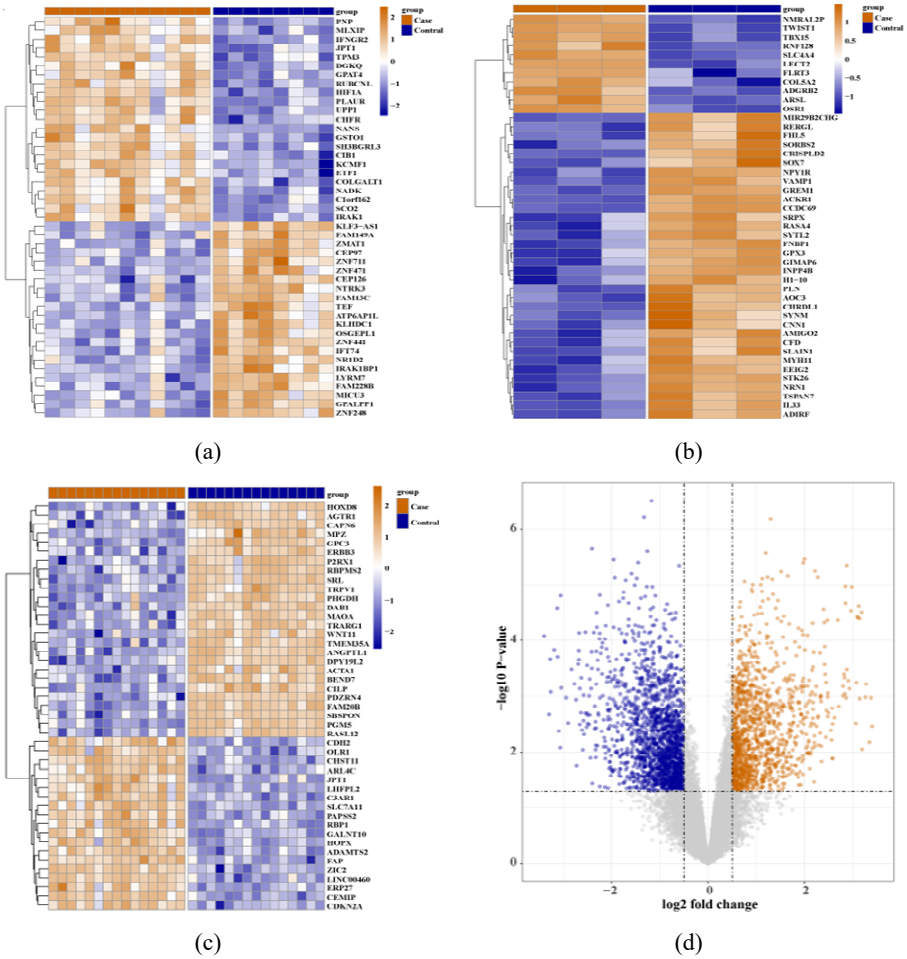

(a) (b)

(c) (d)

Figure 3 Visualisation results of differential analyses within IA rupture progression, (a) the heatmap of differentially expressed genes for GSE13353, (b) GSE26969, (c) GSE75436, (d) GSE13353, (e) GSE26969, (f) the volcano of differentially expressed genes for GSE75436 (continued) (see online version for colours)

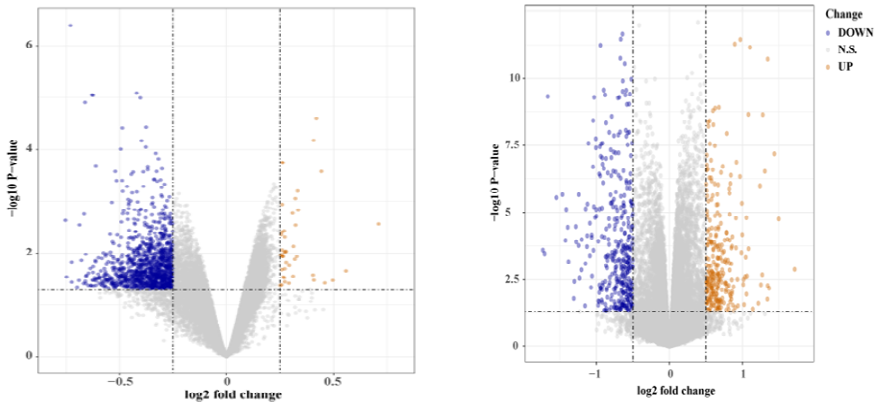

(e) (f)

Differential expression analysis revealed 4,006, 1,208, and 2,344 genes in the GSE13353, GSE26969, and GSE75436 datasets, respectively. Clustering analysis and expression abundance of DEGs across all three GEO datasets were displayed in corresponding heatmaps [Figures 3(a)–3(c)], while volcano plots were employed to visualise these differentially expressed genes (DEGs) [Figures 3(d)–3(f)].

3.2 Identification of hub genes and shared genes

Overlaps among the four datasets were visualised by using Venn diagrams (Figure 3). Specifically, a total of 15, 10, and 14 hub genes overlapping with the 'Diff_Snp_Genes' dataset were identified in the GSE13353, GSE26969, and GSE75436 datasets, respectively. After deduplication, 31 unique hub genes were retained. Furthermore, two genes (ITGAX and MAGI2) were defined as the shared intersection across all four datasets, including 'Diff_Snp_Genes' and DEGs from the three GEO datasets (GSE13353, GSE26969, GSE75436) (Figure 4).

3.3 Enrichment analyses for hub genes

To further elucidate the biological functions of the identified hub genes, we performed GO and KEGG enrichment analyses. GO enrichment and KEGG pathway analyses were performed on the 31 hub genes. The top three enriched biological processes (BP) were plasma membrane bounded cell projection organisation, cell projection organisation, and small GTPase-mediated signal transduction. For cellular components (CC), the most enrichments were plasma membrane bounded cell projection, cell projection, and plasma membrane region. The top three enriched molecular functions (MF) were GTPase regulator activity, nucleoside-triphosphatase regulator activity, and hexosyltransferase activity [Figure 5(a)]. Regulation of actin cytoskeleton emerged as the top KEGG pathway [Figure 5(b)]. However, none of these enrichment results showed statistical significance.

Figure 4 Venn diagram for the 31 hub genes and 2 shared genes (see online version for colours)

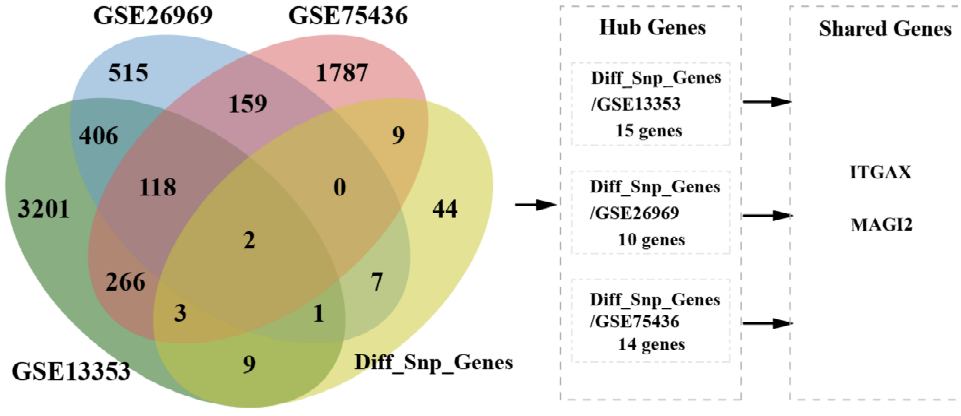

Figure 5 Enrichment analyses for 31 hub genes, (a) the GO enrichment analysis on 31 hub genes. (b) the KEGG pathway enrichment analysis on 31 hub genes (see online version for colours)

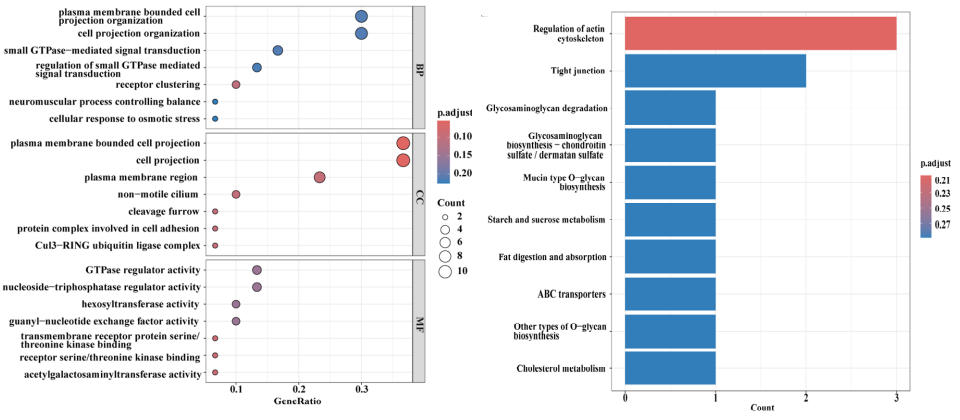

(a) (b)

3.4 *Construction of genes-TF-miRNA interaction network*

Meanwhile, PPI network among the 31 hub genes were explored by using STRING (v12.0). Two interactional gene pairs, ITGAX-JAM3 and KLHL28-TOGARAM1, were identified after applying a confidence threshold = 0.4 [Figure 6(a)]. By integrating these interactional genes with the two shared genes (ITGAX, MAGI2), a refined 'core genes' dataset comprising five genes (ITGAX, JAM3, KLHL28, TOGARAM1, MAGI2) was established. To further reveal regulatory mechanisms among core genes, transcription factors (TFs), and miRNAs, a gene-TF-miRNA coregulatory interaction network was constructed through network analyst (v 3.0). This network included 12 nodes and 16 edges [Figure 6(b)].

Figure 6 Screening and refinement of 'core genes' and the gene-TF-miRNA coregulatory interaction network, (a) the PPI network of 31 hub genes, (b) TF-miRNA coregulatory interaction network on 'core genes' (see online version for colours)

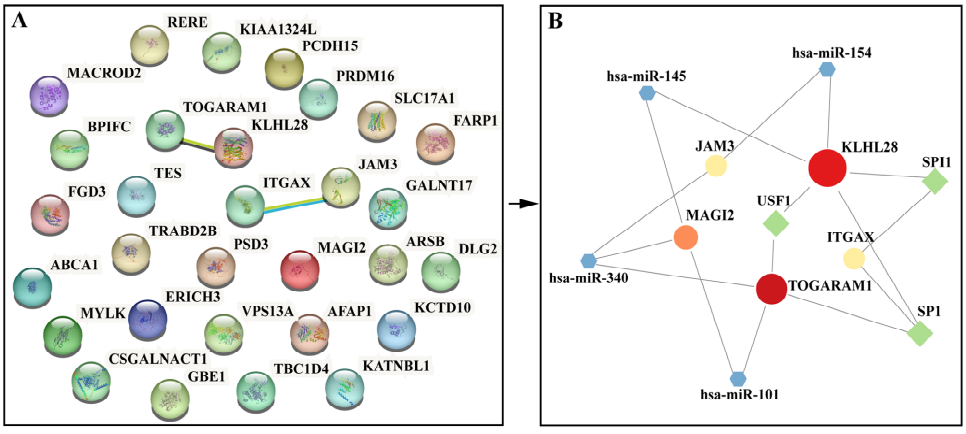

Figure 6 Contruction of a LASSO regression-based predictive model and roc curve-based assessment of predictive power, (A1–A3) selection of optimal λ through LASSO cross-validation on hub, core, and shared gene models. The value in the middle of the two dotted lines is the range of the positive and negative standard deviations of log(λ), (B1–B3) LASSO coefficient profiles for hub, core, and shared gene models, coefficients were standardised, (C1–C3) ROC curve analysis for hub, core, and shared gene predictive models (see online version for colours)

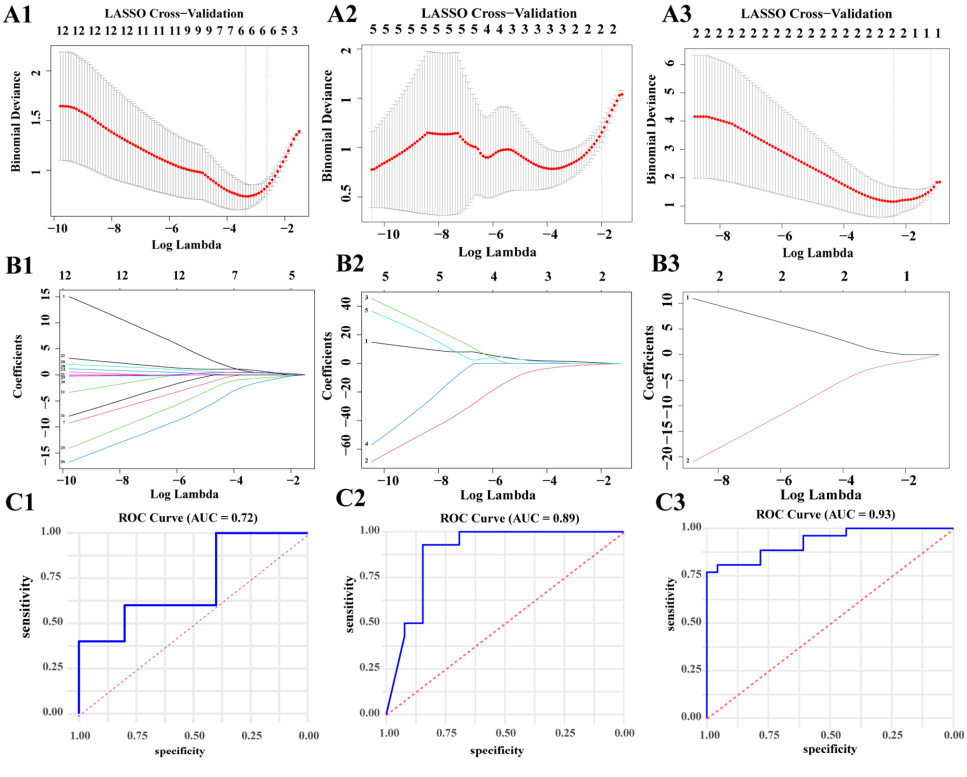

3.5 Predictive model for IA rupture progression

Clinical data from 55 patients (29 cases and 26 controls) were pooled from three GEO datasets. The training set included 15 cases and 13 controls, with the remaining samples allocated to the testing set. We selected the 31 hub genes, 5 core genes, and 2 shared genes as features to plot the relevance of binomial deviance curves against log(λ), further identifying the optimal λ value for the LASSO regression model through 10-fold cross-validation [Figure 7(A1–A3)]. Hub genes model: The optimal λ was 0.04, having five non-zero coefficients (value): ITGAX (0.70), MAGI2 (–1.74), ARSB (0.39), SLC17A1 (0.80), and MACROD2 (–0.56). Core genes model: The optimal λ was 2.87 × 1E-04, identifying five non-zero coefficients (value): ITGAX (0.79), MAGI2 (–1.60), KLHL28 (0.57), TOGARAM1 (–1.75), and JAM3 (0.93). Shared genes model: The optimal lambda λ was 0.09, with two non-zero coefficients (value): ITGAX (0.26) and MAGI2 (–1.83) [Figure 7(B1–B3)]. In addition, ROC curve analysis revealed area under the curve (AUC) values of 0.72, 0.89, and 0.93 for the hub, core, and shared genes models, respectively [Figure 7 (C1–C3)]. These findings suggest a potential role of core genes, particularly the shared genes, in predicting IA rupture.

4 Discussion

The ruptured IA may result in subarachnoid bleeding, vasospasm of cerebral arteries, and various neurological impairments (Wahood et al., 2022; Mualem et al., 2022). However, the pathological mechanisms underlying IA rupture remain incompletely understood. We integrated multidimensional bioinformatics data – including genome-wide association study (GWAS) datasets and transcriptomic profiles – to identify overlapping genes across multiple datasets at present study. Through enrichment analysis, gene-TF-miRNA interaction networks, LASSO regression-based predictive modelling, and ROC curve evaluation, we aimed to theoretically identify novel molecular targets implicated in IA rupture. Among 31 hub genes identified, the interactions between ITGAX-JAM3 and KLHL28-TOGARAM1 were highlighted. Notably, ITGAX and MAGI2, as overlapping genes across multiple datasets, demonstrated robust predictive performance for IA rupture.

ITGAX, also known as CD11c, forms part of the integrin αXβ2 complex and facilitates intercellular communication during inflammatory processes, including the adhesion and migration of monocytes (Hou et al., 2025). Although a direct association between ITGAX and IA rupture has not been established, abnormal expression of this gene is known to participate in the angiogenesis observed in tumours (Oliveira et al., 2010; et al., 2019) and abdominal aortic aneurysm progression (Okuno et al., 2020), suggesting a plausible role in IA pathogenesis. Bioinformatics analyses further support ITGAX as a candidate gene for IA rupture (Chen et al., 2024; Zhang et al., 2023). JAM3 (JAM-C), a protein belonging to the junctional adhesion molecule family, is essential for maintaining endothelial barrier function and controlling the movement of leukocytes across the endothelium, thereby contributing to vascular stability and the regulation of inflammation (Chavakis et al., 2004; Aurrand-Lions et al., 2005; Lamagna et al., 2005;Orlova et al., 2006; Coxon et al., 1996). Zimmerli et al. (2009) experimentally validated the interaction between ITGAX and JAM3. Collectively, both genes are implicated in immune regulation and cell adhesion. Current evidence supports their

potential synergistic interaction in exacerbating inflammatory responses and vascular wall remodelling during IA rupture, thereby influencing disease progression. However, these findings warrant further functional validation to elucidate their mechanistic contributions.

KLHL28 (Kelch-like family member 28), a member of the Kelch family, was first identified in this study to exhibit differential expression during IA rupture. While KLHL28 has not been explicitly studied in the context of IAs, related proteins in the Kelch family (e.g., KLHL2, KLHL3) influence vascular tone and blood pressure via ubiquitination, hinting at a possible function for KLHL28 (Zeniya et al., 2015; Yoshida et al., 2018; Abdel Khalek et al., 2019). Long-standing hypertension increases the vulnerability of vascular tissues at branching points, lowering rupture thresholds (Claassen and Park, 2022). There is no substantial evidence to explain how the KLHL28 affects IA rupture, but we cannot rule out the possibility that KLHL28 may also affect IA rupture by participating in ubiquitination and affecting blood pressure homeostasis. TOGARAM1 has primarily been investigated in relation to ciliopathic disorders. For example, Latour et al. (2020) identified TOGARAM1 as a gene responsible for Joubert syndrome and associated with failures in neural tube closure, often leading to encephaloceles stemming from cranial mesodermal defects (Wang et al., 2025). Notably, chronic hypertension appears to critically exacerbate both encephalocele and cerebrovascular wall protrusion (e.g., IA formation). Theoretical extrapolation suggests that the interplay between KLHL28 and TOGARAM1 may be closely linked to hypertension-driven vascular pathology. However, their functional relationship and disease relevance demand comprehensive investigations, including molecular validation and in vivo studies. MAGI2 (membrane-associated guanylate kinase, WW, and PDZ domain-containing 2) remains understudied in IA research. However, its antisense transcript MAGI2-AS3 exhibits strong expression correlation with MAGI2. Recent findings indicate that the long non-coding RNA MAGI2-AS3 may modulate MAGI2 function via cis-acting mechanisms, including epigenetic alterations (Xu et al., 2021). Given the critical role of endothelial barrier dysfunction in IA rupture, dysregulation of MAGI2-dependent cell-cell signalling pathways may contribute to vascular destabilisation.

5 Limitations

This study has several limitations that should be considered when interpreting the findings. First, the mechanistic insights for the novel candidate genes proposed (e.g., KLHL28, TOGARAM1) are primarily derived from bioinformatic inferences and indirect evidence. Future work will include functional validation of these targets in hypertensive animal models, as well as analysis of the correlation between the expression of these genes and blood pressure levels in clinical cohorts. Second, the predictive performance of our genomic model, although robust in our internal cohort, requires further evaluation. The absence of external validation in an independent dataset, constrained by the limited public availability of suitable RNA-seq data, affects the assessment of its generalisability. It is also important to emphasise that the primary goal of this model was not immediate clinical prediction, but rather to prioritise the most promising candidate genes from a large set for further biological experimentation – thereby helping to focus subsequent research efforts efficiently. Finally, these limitations underscore the challenge of

investigating novel targets with limited prior functional annotation and research resources. Our immediate priority is to secure dedicated funding to enable functional validation in hypertensive animal models and correlation studies in clinical cohorts, a critical imperative for advancing these discoveries toward therapeutic applications.

6 Conclusions

This study reveals novel molecular interactions and potential regulatory mechanisms underlying IA rupture, highlighting their association with inflammatory responses and hypertension-related vascular remodelling. These findings lay a molecular foundation for exploring hypertension-driven mechano-immune crosstalk and developing dual-action therapeutic strategies that integrate antihypertensive and anti-inflammatory properties. While bioinformatics and machine learning approaches predicted the therapeutic potential of these targets (ITGAX, JAM3, KLHL28, TOGARAM1, and MAGI2), the lack of direct experimental evidence, which is attributable to the unprecedented nature of these associations, signposts critical directions for future research, particularly in functional validation and mechanistic exploration.

Acknowledgments

We acknowledge the contributions by Sakaue S et al. for performing the original GWASs and for making summary statistics data publicly available, as well as by IEU Open GWAS project. And we also thank the contributions by Kurki M et al., Liu D et al., and Yu L et al. for making original Series Matrix Files, as well as by GEO database.

Declarations

Data availability statement: the raw data supporting the conclusions of this article will be made available by the authors, without undue reservation.

Ethics statement: summary statistics for UIA (ebi-a-GCST90018816) and IA (ebi-a-GCST90018815) were retrieved from the IEU Open GWAS Project (https://gwas.mrcieu.ac.uk/). Three datasets (GSE13353, GSE26969, and GSE75436) were all from GEO database (https://www.ncbi.nlm.nih.gov/gds/). As all datasets were sourced from publicly available repositories, no additional ethical approval was required.

Funding statement: the authors received no financial support for the research, authorship, and/or publication of this article.

Conflict of interest: the authors declare that the research was conducted in the absence of any commercial or financial relationships that could be construed as a potential conflict of interest.

References

Abdel Khalek, W., Rafael, C., Loisel-Ferreira, I., Kouranti, I., Clauser, E., Hadchouel, J. and Jeunemaitre, X. (2019) 'Severe arterial hypertension from Cullin 3 mutations is caused by both renal and vascular effects', *J. Am. Soc. Nephrol*., Vol. 30, pp.811–823.

Aurrand-Lions, M., Lamagna, C., Dangerfield, J.P., Wang, S., Herrera, P., Nourshargh, S. and Imhof, B.A. (2005) 'Junctional adhesion molecule-C regulates the early influx of leukocytes into tissues during inflammation', *J. Immunol.*, Vol. 174, pp.6406–6415.

Bor, A.S., Rinkel, G.J., Van Norden, J. and Wermer, M.J. (2014) 'Long-term, serial screening for intracranial aneurysms in individuals with a family history of aneurysmal subarachnoid haemorrhage: a cohort study', *Lancet Neurol*., Vol. 13, pp.385–392.

Bor, A.S., Velthuis, B.K., Majoie, C.B. and Rinkel, G.J. (2008) 'Configuration of intracranial arteries and development of aneurysms: a follow-up study', *Neurology*, Vol. 70, pp.700–705.

Chavakis, T., Keiper, T., Matz-Westphal, R., Hersemeyer, K., Sachs, U.J., Nawroth, P.P., Santoso, S. (2004) 'The junctional adhesion molecule-C promotes neutrophil transendothelial migration in vitro and in vivo', *J. Biol. Chem.*, Vol. 279, p.55602-8.

Chen, Y., Huang, J.H., Kang, Y.B., Yao, Z.J. and Song, J.H. (2024) 'Bioinformatics analysis revealed the potential crosstalk genes and molecular mechanisms between intracranial aneurysms and periodontitis', *BMC Med. Genomics*, Vol. 17, p.114.

Claassen, J. and Park, S. (2022) 'Spontaneous subarachnoid haemorrhage', *Lancet*, Vol. 400, pp.846–862.

Coxon, A., Rieu, P., Barkalow, F.J., Askari, S., Sharpe, A.H., Von Andrian, U.H., Mayadas, T.N. (1996) 'A novel role for the beta 2 integrin CD11b/CD18 in neutrophil apoptosis: a homeostatic mechanism in inflammation', *Immunity*, Vol. 5, pp.653–666.

Etminan, N. and Rinkel, G.J. (2016) 'Unruptured intracranial aneurysms: development, rupture and preventive management', *Nat. Rev. Neurol*., Vol. 12, No. 5, pp.699–713.

Etminan, N., Buchholz, B.A., Dreier, R., Bruckner, P., Torner, J.C., Steiger, H.J. and Macdonald, R.L. (2014) 'Cerebral aneurysms: formation, progression, and developmental chronology', *Transl. Stroke Res.*, Vol. 5, No. 2, pp.167–173.

Etminan, N., Chang, H.S., Hackenberg, K., De Rooij, N.K., Vergouwen, M.D.I., Rinkel, G.J.E. and Algra, A. (2019) 'Worldwide incidence of aneurysmal subarachnoid hemorrhage according to region, time period, blood pressure, and smoking prevalence in the population: a systematic review and meta-analysis', *JAMA Neurol*., Vol. 76, No. 5, pp.588–597.

Frösen, J., Tulamo, R., Heikura, T., Sammalkorpi, S., Niemelä, M., Hernesniemi, J., . . . YLä-Herttuala, S. (2013) 'Lipid accumulation, lipid oxidation, and low plasma levels of acquired antibodies against oxidized lipids associate with degeneration and rupture of the intracranial aneurysm wall', *Acta Neuropathol. Commun*., Vol. 1, No. 1, p.71.

Frösen, J., Tulamo, R., Paetau, A., Laaksamo, E., Korja, M., Laakso, A., . . . Hernesniemi, J. (2012) 'Saccular intracranial aneurysm: pathology and mechanisms', *Acta Neuropathol*., Vol. 123, No. 6, pp.773–786.

Hou, L., Koutsogiannaki, S. and Yuki, K. (2025) 'Multifaceted, unique role of CD11c in leukocyte biology', *Front Immunol*., Vol. 16, No. 4, p.1556992.

Huang, J., Yang, L. and Lin, Y.Z. (2024) 'Uncovering the intension of Alisma orientale decoction for treating vertigo: a perspective from network analysis', *International Journal of Data Mining and Bioinformatics*, Vol. 28, No. 1, pp.58–72.

Kassam, A., Horowitz, M., Chang, Y.F. and Peters, D. (2004) 'Altered arterial homeostasis and cerebral aneurysms: a review of the literature and justification for a search of molecular biomarkers', *Neurosurgery*, Vol. 54, No. 5, pp.1199–1111, discussion 1211-2.

Lamagna, C., Meda, P., Mandicourt, G., Brown, J., Gilbert, R.J., Jones, E. Y., . . . Aurrand-Lions, M. (2005) 'Dual interaction of JAM-C with JAM-B and alpha(M)beta2 integrin: function in junctional complexes and leukocyte adhesion', *Mol. Biol. Cell*, Vol. 16, No. 10, pp.4992–5003.

Latour, B.L., Van De Weghe, J.C., Rusterholz, T.D., Letteboer, S.J., Gomez, A., Shaheen, R. and Doherty, D. (2020) 'Dysfunction of the ciliary ARMC9/TOGARAM1 protein module causes Joubert syndrome', *J. Clin. Invest*, Vol. 130, No. 10, pp.4423–4439.

Mualem, W., Durrani, S., Ghaith, A.K., Bhandarkar, A.R., Wahood, W., Tjoumakaris, S. and Bydon, M. (2022) 'Factors associated with increased inpatient charges following aneurysmal subarachnoid hemorrhage with vasospasm: a nationwide analysis', *Clin. Neurol. Neurosurg.*, Vol. 218, No. 1, p.107259.

Muller, M., Van Den Beld, A.W., Bots, M.L., Grobbee, D.E., Lamberts, S.W. and Van Der Schouw, Y.T. (2004) 'Endogenous sex hormones and progression of carotid atherosclerosis in elderly men', *Circulation*, Vol. 109, No. 1, pp.2074–2079.

Okuno, K., Cicalese, S. and Eguchi, S. (2020) 'Depletion of CD11c+ cell attenuates progression of abdominal aortic aneurysm', *Clin. Sci.* (Lond.), Vol. 134, No. 1, pp.33–37.

Oliveira, L.A., Baker, R.K., Klewer, S.E. and Kitten, G.T. (2010) 'Expression of beta 2 integrin (CD18) in embryonic mouse and chicken heart', *Braz. J. Med. Biol. Res.*, Vol. 43, No. 1, pp.25–35.

Orlova, V.V., Economopoulou, M., Lupu, F., Santoso, S. and Chavakis, T. (2006) 'Junctional adhesion molecule-C regulates vascular endothelial permeability by modulating VE-cadherin-mediated cell-cell contacts', *J. Exp. Med.*, Vol. 203, No. 12, pp.2703–2714.

Vlak, M.H., Rinkel, G.J., Greebe, P., Van Der Bom, J.G. and Algra, A. (2011) 'Trigger factors and their attributable risk for rupture of intracranial aneurysms: a case-crossover study', *Stroke*, Vol. 42, No. 7, pp.1878–1882.

Wahood, W., Rizvi, A.A., Alexander, A.Y., Yolcu, Y.U., Lanzino, G., Brinjikji, W. and Rabinstein, A.A. (2022) 'Trends in admissions and outcomes for treatment of aneurysmal subarachnoid hemorrhage in the United States', *Neurocrit Care*, Vol. 37, No. 1, pp.209–218.

Wang, J., Yang, L., Liang, F., Chen, Y. and Yang, G. (2019) 'Integrin alpha x stimulates cancer angiogenesis through PI3K/Akt signalling-mediated VEGFR2/VEGF-A overexpression in blood vessel endothelial cells', *J. Cell Biochem*., Vol. 120, No. 2, pp.1807–1818.

Wang, Y., Kraemer, N., Schneider, J., Ninnemann, O., Weng, K., Hildebrand, M. and Kaindl, A.M. (2025) 'Togaram1 is expressed in the neural tube and its absence causes neural tube closure defects', *HGG Adv*., Vol. 6, No. 1, p.100363.

Xu, X., Yuan, X., Ni, J., Guo, J., Gao, Y., Yin, W. and Zhang, J. (2021) 'MAGI2-AS3 inhibits breast cancer by downregulating DNA methylation of MAGI2', *J. Cell Physiol.*, Vol. 236, No. 2, pp.1116–1130.

Yoshida, S., Araki, Y., Mori, T., Sasaki, E., Kasagi, Y., Isobe, K., . . . Sohara, E. (2018) 'Decreased KLHL3 expression is involved in the pathogenesis of pseudohypoaldosteronism type II caused by cullin 3 mutation in vivo', *Clin. Exp. Nephrol.*, Vol. 22, No. 6, pp.1251–1257.

Zeniya, M., Morimoto, N., Takahashi, D., Mori, Y., Mori, T., Ando, F. and Uchida, S. (2015) 'Kelch-like protein 2 mediates angiotensin ii-with no lysine 3 signalling in the regulation of vascular tonus', *J. Am. Soc. Nephrol.*, Vol. 26, No. 9, pp.2129–2138.

Zhang, Q., Liu, H., Zhang, M., Liu, F. and Liu, T. (2023) 'Identification of co-expressed central genes and transcription factors in atherosclerosis-related intracranial aneurysm', *Front Neurol*., Vol. 14, No. 2, p.1055456.

Zimmerli, C., Lee, B.P., Palmer, G., Gabay, C., Adams, R., Aurrand-Lions, M. and Imhof, B.A. (2009) 'Adaptive immune response in JAM-C-deficient mice: normal initiation but reduced IgG memory', *J. Immunol.*, Vol. 182, No. 8, pp.4728–4736.